

Pitch Carbon-coated Ultrasmall Si Nanoparticle Lithium-ion Battery Anodes Exhibiting Reduced Reactivity with Carbonate-based Electrolyte

Maxwell C. Schulze,^{*[a]} Kae Fink,^[a] Jack Palmer,^[a] Gerard M. Carroll,^[a] Nikita S. Dutta,^[a] Christof Zwiefel,^[a] Chaiwat Engtrakul,^[a] Sang-Don Han,^[a] Nathan R. Neale,^[a] and Bertrand J. Tremolet de Villers^[a]

Silicon anodes for lithium-ion batteries (LIBs) have the potential for higher energy density compared to conventionally used graphite-based LIB anodes. However, silicon anodes exhibit poor cycle and calendar lifetimes due to mechanical instabilities and high chemical and electrochemical reactivity with the carbonate-based electrolytes that are typically used in LIBs. In this work, we synthesize a pitch carbon-coated silicon nanoparticle composite active material for LIB anodes that exhibits reduced chemical reactivity with carbonate-based electrolytes compared to an uncoated silicon anode. Silicon primary particle sizes less than 10 nm diameter minimize micro-scale mechanical

degradation of the anode composite, while conformal coatings of pitch carbon minimize the parasitic reactions between the silicon and the electrolyte. When matched with a high voltage NMC622 ($\text{LiNi}_{0.6}\text{Mn}_{0.2}\text{Co}_{0.2}\text{O}_2$) cathode, the pitch carbon-coated silicon anode retains $\approx 75\%$ of its initial capacity at the end of 1000 cycles. Increasing the areal loading of the pitch carbon-coated silicon anodes to realize energy density improvements over graphite anodes results in severe mechanical degradation on the electrode level, highlighting a remaining challenge to be addressed in future work.

Introduction

Silicon (Si) is one of the most studied materials for use in next generation lithium-ion batteries (LIBs) due to its ability to store high capacities of lithium compared to graphite.^[1] However, even after decades of study, it remains challenging to commercially produce LIBs with majority-Si anodes that can deliver competitive cycle and calendar lifetimes and improved energy densities compared to state-of-the-art graphite-based LIBs. One major challenge hindering Si anodes is the greater than 3× volume change between lithiated and delithiated states that causes mechanical degradation, active material isolation, mechanical destabilization of passivating solid-electrolyte-interphase (SEI) layers, and ultimately rapid capacity loss.^[2] Previous studies have identified particle size thresholds around 150 nm, above which Si particles will crack and pulverize during cycling, causing continuous SEI disruption and regrowth.^[3] Most recent studies have thus focused on Si anodes made with nano-sized Si,^[4] despite micron-sized Si being significantly less expensive and easier to process.

A second major challenge limiting performance of Si anodes is a high chemical reactivity between the Si active material and carbonate-based electrolytes, resulting in poorly passivating SEI

layers and a variety of other deleterious effects.^[5] In fact, *ex situ* studies have shown that cycling Si electrodes in carbonate-based electrolytes will cause the SEI to grow into the Si active material, forming heterogenous Si-SEI composites rather than a passivating SEI shell forming on Si particles.^[6] This suggests that even electrodes with Si dimensions small enough to avoid cracking (e.g., ~ 100 nm) will eventually reach configurations where Si features less than 10 nm are thoroughly intermixed with SEI components. Such a transformation consumes a significant amount of electrochemically active Li inventory and electrolyte and results in loss of active material through dissolution or isolation of Si domains.

To address both of these issues, Si active materials should be designed to avoid particle cracking through use of nanoscale Si while simultaneously minimizing the deleterious chemical reactions between the Si and the electrolyte. Such design principles may seem at odds with each other, as smaller particles means that more Si surface area will be in contact with the electrolyte. However, these competing effects can be managed by coating appropriately small Si particles with a medium that minimizes direct Si-electrolyte contact while still allowing Li-ion and electron conduction to and from the Si. Many of the commonly researched Si-carbon composite active materials prevent Si-electrolyte contact to some extent,^[7] although most have Si particle sizes greater than 10 nm that will result in the detrimental transformation to smaller Si domains when unavoidable electrolyte contact occurs during cycling. There are examples of materials that satisfy the criteria of both appropriately small Si particles of less than 10 nm and with carbon-coatings,^[8] including a promising material that is synthesized by impregnating a micron sized nano-porous

[a] Dr. M. C. Schulze, K. Fink, J. Palmer, Dr. G. M. Carroll, Dr. N. S. Dutta, C. Zwiefel, Dr. C. Engtrakul, Dr. S.-D. Han, Dr. N. R. Neale, Dr. B. J. Tremolet de Villers
National Renewable Energy Laboratory
15013 Denver West Parkway, 80401 Golden, CO (USA)
E-mail: max.schulze@nrel.gov

 Supporting information for this article is available on the WWW under <https://doi.org/10.1002/batt.202300186>

silicon particle with petroleum pitch followed by carbonization.^[9] Our team also has published several examples of alternative approaches based on molecular rather than bulk carbonaceous coatings targeting this strategy,^[10] some of which exhibit highly promising performance.^[11]

Here, we present the fabrication of a Si/pitch composite material that meets the above criteria, where ultrasmall diameter ($d=5.9$ nm) Si nanoparticles (NPs) are coated with pitch carbon to form a Si/pitch composite. Si particles less than 10 nm are not only below the 150 nm threshold identified for single particle fracture but are equivalent to the size that the Si domains will inevitably reach when cycled in a carbonate-based electrolyte. This, in combination with the pitch carbon-coating that acts as a mixed conducting matrix for Li-ion and electron conduction, minimizes direct contact between the Si nanoparticles and electrolyte, thus avoiding the significant chemical and electrochemical degradation that occurs at such an interface. We demonstrate the reduced chemical and electrochemical reactivity of the Si/pitch with a standard carbonate-based electrolyte through measurements of evolved gases and parasitic electrochemical currents, respectively. Electrodes fabricated using the Si/pitch material exhibit long cycle lifetimes when prelithiated and paired against capacity-matched NMC622 cathodes, retaining 75% of their initial capacity over 1000 cycles with minimal impedance increase. Finally, we use high-loading electrodes (greater than 3 mAh/cm²) fabricated using the high-performing Si/pitch active material to highlight macro-mechanical degradation at the electrode level as a remaining challenge for high Si-content electrodes to overcome.

Results and Discussion

Figure 1(a) schematically shows the Si NP pitch carbon-coating. The coating process includes a high-temperature carbonization step at 700 °C. The pitch carbon is comprised of various sp² carbon-rich polycyclic aromatic hydrocarbons,^[12] such as the methyl-benzo[a]pyrene shown in Figure 1(a), which are converted into an amorphous carbon matrix during the carbonization as indicated by the Raman spectrum in Figure S2. We posit that the high temperature process also causes SiH_x surface groups to decompose and off-gas hydrogen, causing surface reconstruction and leaving Si nanoparticle surfaces that are chemically bound to the carbon matrix. A carbonization temperature optimization discussed in the Supporting Information identified 700 °C as the optimal temperature to form an amorphous matrix with mixed sp²+sp³ carbon while preventing formation of silicon carbide, a phase inactive towards lithiation. The composite of the Si NPs in the carbon matrix are then milled down to the Si/pitch powder used as the active material for electrochemical studies. Characterization of the Si/pitch powder discussed in the Supporting Information reveals it has a surface area around 5 m²/g and an elemental composition of 60%–70% Si, 27%–36% C, ~3% O, 0.2% N, 0.8% H, and 0.1% S by mass. Analysis of the powder by transmission electron microscopy (TEM) (Figure 1b) reveals it has micron-scale secondary particles comprised of less than 10 nm Si NPs aggregated in the carbon matrix (see Figure S3 for additional TEM micrographs and Figure S4 for energy dispersive X-ray spectroscopy (EDS) maps of the Si/pitch powder). We hypothesize that this morphology provides several advantages when used as an active material in a Li-ion battery anode:

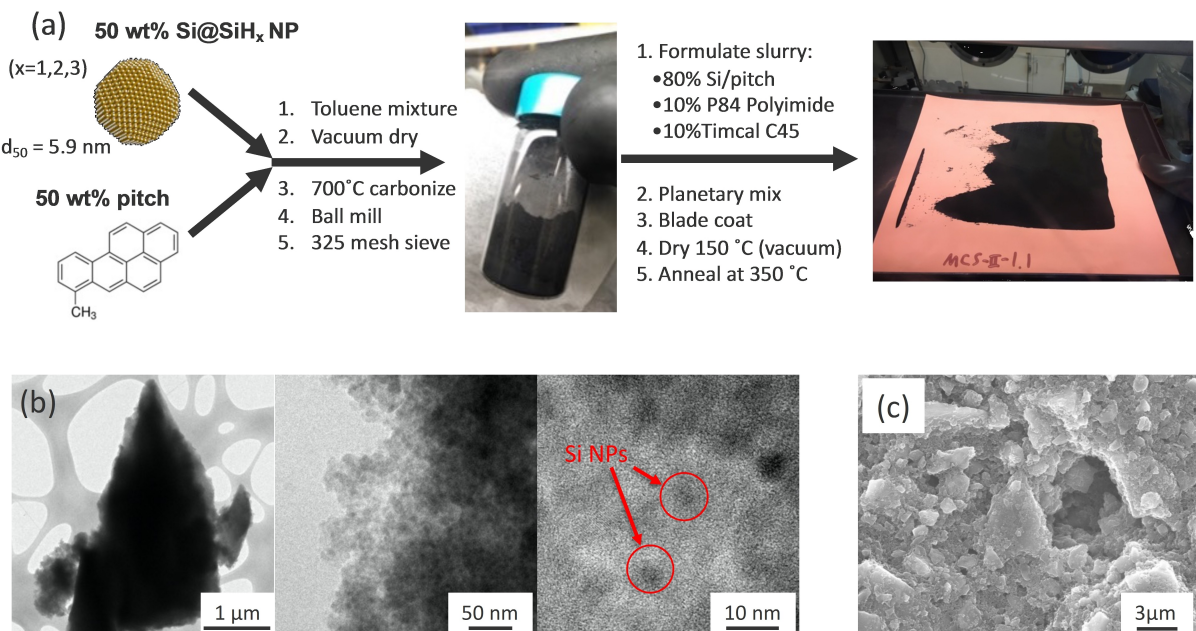


Figure 1. a) Synthesis schematic of the Si/pitch powder, and subsequent fabrication into a composite electrode via slurry casting. b) TEM micrographs of the Si/pitch powder showing less than 10 nm Si primary particles (highlighted in red) in a pitch carbon matrix made of greater than 1 μm size secondary particles. c) Top-down scanning electron microscopy (SEM) micrograph of the Si/pitch composite electrode with micron scale pore sizes.

- 1) The ultra-small (less than 10 nm) Si prevents Si particle cracking or other processes that expose additional surface area to the battery electrolyte during electrochemical cycling.^[13]
- 2) The micron-scale secondary particles minimize electroactive surface area exposed to the electrolyte compared to an electrode made with unaggregated and uncoated Si NPs. This minimizes both chemical and electrochemical side reactions between the electrode and electrolyte.

The chemical reactivity of both uncoated Si NPs and carbon-coated Si/pitch active materials with the GenF3 electrolyte (1.2 M lithium hexafluorophosphate (LiPF_6) in 3:7 ethylene carbonate:ethylmethyl carbonate + 3 wt.% fluoroethylene carbonate, less than 10 ppm water content) was assessed. Figure S5 schematically describes our method to collect and identify evolved gases using gas-chromatography with a flame-ionization detector (GC-FID). The major gas species evolved included CH_4 , C_2H_4 , and C_2H_6 , which were identified through calibration against standard gas samples. In prior work, we have shown that ethylene gas (C_2H_4) in particular is a product of the chemical reaction between the uncoated Si NPs and the ethylene carbonate in the electrolyte.^[14] Figure 2(a) shows the total integrated quantities per milligram of Si of each of the gasses produced when soaking the active material powders in the GenF3 electrolyte. The substantially greater amount of ethylene gas produced by the uncoated Si NP active material powder compared to the Si/pitch powder indicates that the pitch coating helps to minimize the chemical reactivity between

Si and the GenF3 electrolyte. Both uncoated Si NPs and Si/pitch powders were fabricated into composite electrodes by traditional slurry casting techniques as described in the Experimental section. The amount of gas produced by each material becomes more comparable when soaking the prepared electrodes of each the uncoated Si NPs and Si/pitch in the GenF3 electrolyte (Figure 2b), indicating that the electrode processing itself may mitigate some of the chemical reactivity. However, the electrochemical reactivity of each material also determines how well each will perform in a practical battery.

Electrochemical analysis indicates that the pitch carbon-coating of the Si NPs significantly reduces the anode's electrochemical reactivity with the electrolyte. Punches from each electrode were assembled into half-cells, and voltage holds were used to assess how the pitch carbon-coating affected the electrochemical reactivity of the active materials in a fully lithiated state. Figure 3(a) shows the potential profiles of the voltage hold (at 10 mV vs. Li/Li^+) experiment run on the uncoated Si NP and Si/pitch electrodes while Figure 3(b) shows the current response of each measured during the 180 h voltage hold step. This protocol serves as a qualitative comparison tool between different electrode materials, where the residual currents measured at the end of the long voltage hold are related to the parasitic current due to electrochemical side reactions at the electrode-electrolyte interface.^[15] The smaller residual current value measured for the Si/pitch electrode compared to the uncoated Si NP electrode indicate that the pitch coating process is lowering the electrochemical

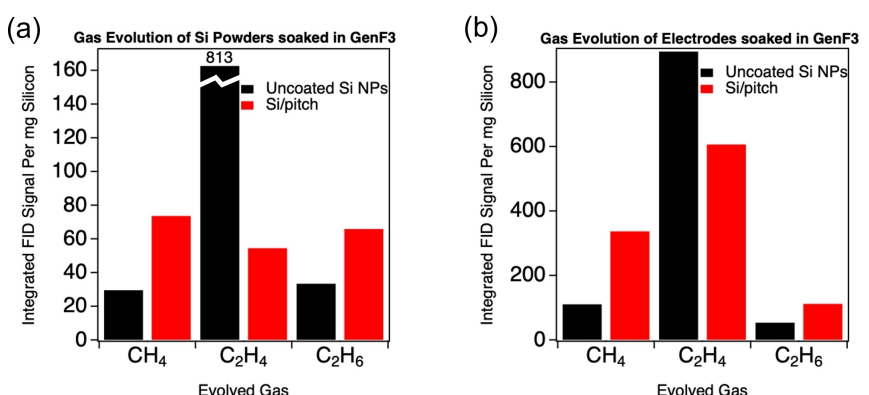


Figure 2. Chemical reactivity between the Si containing materials and the electrolyte was evaluated by measuring the integrated GC-FID signals of various gasses (CH_4 , C_2H_4 , and C_2H_6) evolved from soaking either a) the active material powders or b) electrode scraps in the carbonate-based electrolyte.

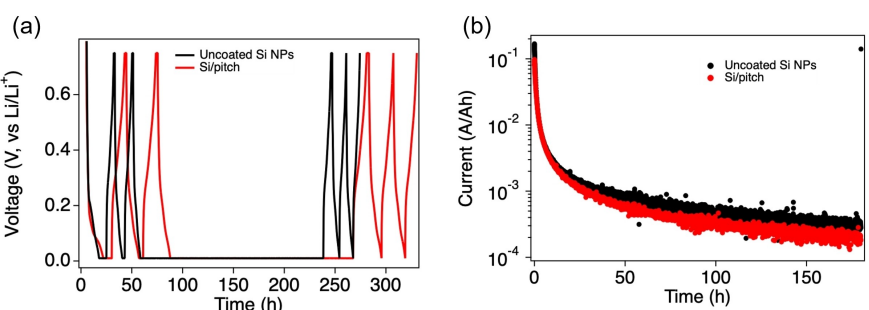


Figure 3. a) Voltage profiles and b) current decay during 180 h voltage hold at 10 mV.

reactivity of the Si active material with the carbonate-based electrolyte.

The reduced chemical and electrochemical reactivity of the carbon-coated Si/pitch with the electrolyte indicates that the active material should exhibit good performance in a full-cell. Specifically, minimized side reactions should slow Li-inventory consumption and concomitant capacity loss in a capacity-matched full-cell while also slowing SEI growth and concomitant growth of impedance. Because repeated cycling of Si electrodes causes significant volume changes and associated mechanical strain during lithiation and delithiation, an additional annealing step was performed on the Si/pitch electrode prior to full-cell cycling to improve the electrochemical performance (see Figure S6 for electrochemical results of a Si/pitch electrode that did not undergo this additional annealing step).^[16] Additionally, the Si/pitch electrode was pre-cycled in a half-cell prior to assembly in a Si/pitch || NMC622 full-cell to account for the irreversible losses on the first few cycles associated with forming the SEI (see Figure 4a). While such a method for “pre-lithiating” or “pre-forming” a silicon electrode in a half-cell and harvesting it for a full-cell is tractable for research studies, it is impractical for larger format, multi-layer, or commercial cells. The development of pre-lithiation methods for practical production scale is the focus of continuing studies. A pre-formed Si/pitch electrode was harvested from the half-cell and matched against an NMC622 cathode in a full-cell and underwent an initial rate capability test, as shown in Figure 4b.

The rate capability experiment indicated that the Si/pitch || NMC622 full-cell can be cycled as fast as 1 C with minimal capacity fade. Thus, a different pre-formed Si/pitch electrode was cycled in a NMC622 full-cell at 1 C for 1000 cycles, with periodic reference performance tests (RPTs) comprising a few slower cycles at a C/3 rate and a hybrid pulsed power characterization (HPPC) test.^[17] The long-term cycling data in Figure 4(c) shows that the Si/pitch-NMC622 cell exhibits a capacity retention of ~75% after 1000 cycles where the 1 C cycles have an average coulombic efficiency of 99.91%. A corresponding uncoated Si electrode full-cell was not tested in this work because our previous work indicated such poor performance of uncoated Si even when tested in a half-cell configuration.^[18]

Analysis of the HPPC test data during the RPTs is shown in Figure 4(d). Discharge area-specific impedance (ASI) values begin around $15 \Omega/\text{cm}^2$ at high cell potentials (above 3.3 V cell potential) and remain below $20 \Omega/\text{cm}^2$ over the 1000 cycles. The ASI values below 3.3 V cell potential exhibit a decreasing trend, starting high around $60 \Omega/\text{cm}^2$ and decreasing to around $30 \Omega/\text{cm}^2$. This decreasing ASI trend at low cell potentials is likely driven by cathode impedance, where high states of cathode lithiation at the beginning of life result in a larger impedance. As the lithium inventory is irreversibly lost in the cell, the cathode reaches progressively less lithiated states, resulting in a smaller impedance. The ASI values above 3.3 V cell potential are smaller than those of Si-NMC cells reported

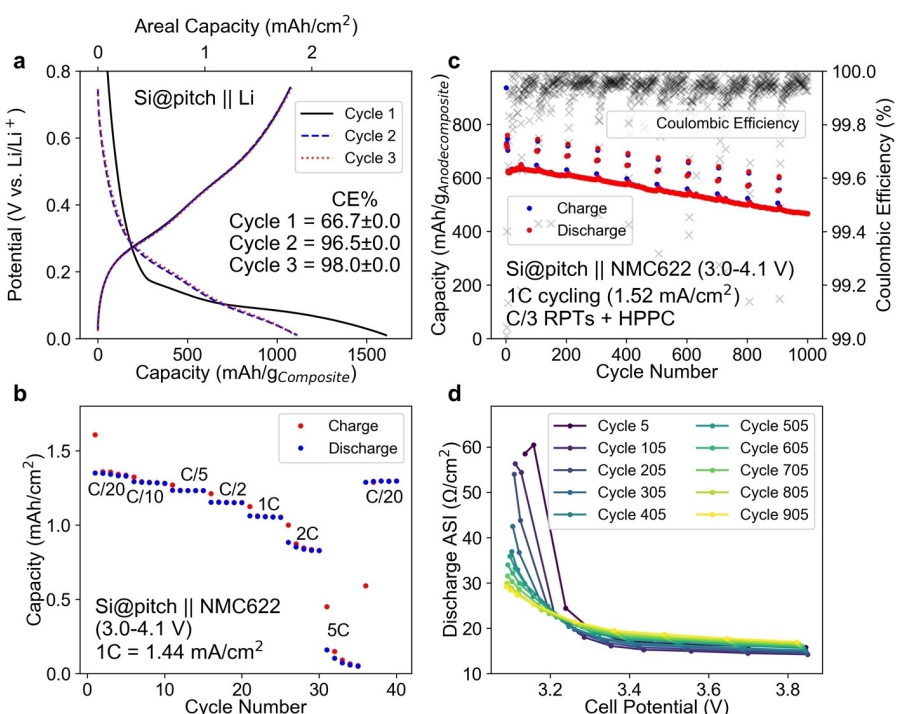


Figure 4. a) Voltage vs. capacity plots measured during formation of a Si@pitch electrode in a half-cell. Following formation in the half-cell, Si@pitch electrodes were recovered and reassembled into a full-cell against an NMC622 cathode for further electrochemical testing. **b)** Long-term cycling performance of a Si@pitch || NMC622 full-cell that was cycled between 3.0–4.1 V vs. Li/Li⁺. The testing protocols comprises 1 C rate cycling with periodic reference performance tests (RPTs) every 100 cycles, each comprising 5× cycles at a C/3 rate with an HPPC protocol during the final RPT discharge that is detailed in the experimental. **c)** A rate capability test of a Si@pitch || NMC622 full-cell. **d)** Area-specific impedance (ASI) calculated from the HPPC protocol run during each RPT of the long-term cycling of a Si@pitch || NMC622 full-cell.

elsewhere, where ASI values can be greater than $30 \Omega/\text{cm}^2$ at beginning of life and can increase up to $50 \Omega/\text{cm}^2$ impedance.^[19] These analyses indicate that the pitch carbon-coating of the Si NPs is effectively minimizing impedance rise from excessive SEI growth by protecting the Si from side reactions with the electrolyte.

Despite the promising full-cell cycling performance of Si/pitch electrodes, future work is required to address the electrode-level mechanical degradation issues that many high-loading Si electrodes exhibit.^[20] To realize improvements in battery energy density by using Si active material, electrodes with high areal loadings need to deliver $3\text{--}5 \text{ mAh}/\text{cm}^2$ of capacity. Figure 5(a) shows calculated full-cell stack energy densities for hypothetical Si electrodes paired against NMC cathodes of given areal capacities. The Si/pitch electrode tested in this work is paired against a NMC622 cathode that can deliver $1.49 \text{ mAh}/\text{cm}^2$, which results in a full-cell stack energy density that asymptotes to a theoretical limit around 250 Wh/kg . In comparison, a Si electrode with sufficiently high loading to be paired against a $3\text{--}5 \text{ mAh}/\text{cm}^2$ NMC811 ($\text{LiNi}_{0.8}\text{Mn}_{0.1}\text{Co}_{0.1}\text{O}_2$) cathode could potentially achieve a 350 Wh/kg full-cell stack energy density. However, increasing the anode loading can lead to mechanical instabilities of the electrode, which we detail below.

Electrodes with Si/pitch active material can deliver greater than $3 \text{ mAh}/\text{cm}^2$ in a half-cell (see Figure S7), making Si/pitch a possible material choice for high energy density applications. However, upon disassembly to recover a Si/pitch electrode for reassembly into a full-cell, only shredded electrode pieces, as shown in Figure 5(b), are recovered. We attribute this shredding phenomenon to excessive stress buildup during lithiation of the Si/pitch that ultimately leads to the fracture strain of the Cu current collector being exceeded. Not only does this indicate a high adhesion strength imparted by the P84 polyimide binder (quantification via peel test failed due to inability to remove P84 from Cu foil with another adhesive), but more importantly, that macro-mechanical issues of high-volume change alloy anode materials like Si remain challenges to be solved. Future

work to achieve higher energy density full-cells should focus on developing mitigation strategies for shredding and other macro-mechanical issues like electrode rippling or stretching. A potential strategy could be to engineer higher porosities into composite electrodes to accommodate the active material volume changes. Post-processing methods such as patterning of electrodes via laser ablation is another example of a technique to solve these issues.^[21]

Conclusions

In summary, we have developed a procedure to coat ultrasmall (less than 10 nm diameter) Si nanoparticles with a pitch carbon and fabricate them into composite anodes for Li-ion batteries. The Si/pitch active material powder comprises single-nanometer Si nanoparticles embedded in a conductive carbon matrix to form micron-sized secondary particles. We show that the pitch carbon-coating effectively minimizes chemical reactivity with a carbonate-based electrolyte, as evidenced by reduced C_2H_4 production for Si/pitch relative to uncoated Si. This indicates that the Si/pitch material is a good choice as an active material for a more stable lithium-ion battery anode. The Si/pitch composite electrodes exhibit smaller parasitic currents during voltage holds compared to electrodes made with uncoated Si nanoparticles. Such reduction in voltage-hold currents indicates that the pitch carbon-coating process also reduces electrochemical side-reactions between the Si nanoparticles and the carbonate-based electrolyte that are responsible for short cycle and calendar lifetimes of Si containing electrodes. When prelithiated and matched against an NMC622 cathode, the Si/pitch electrode retains $\sim 75\%$ of its initial capacity after 1000 cycles with minimal impedance rise. When Si/pitch electrodes are fabricated with loadings greater than $3 \text{ mAh}/\text{cm}^2$ to target competitively high full-cell stack energy densities, they begin exhibiting catastrophic macro-mechanical degradation during prelithiation where the Cu current collector becomes shredded. Developing strategies to mitigate shred-

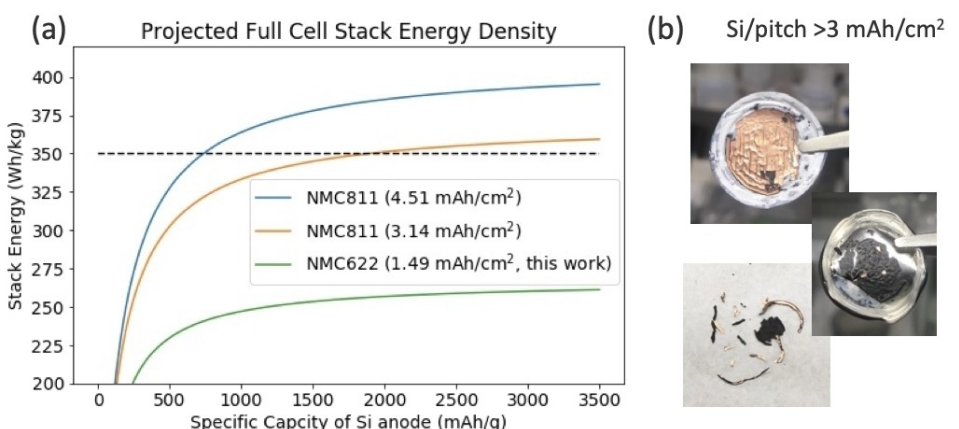


Figure 5. a) Calculated gravimetric energy density of hypothetical Si-NMC full cell stacks. Calculation details can be found in Supporting Information. b) Photographs of Si/pitch electrodes with areal capacities greater than $3 \text{ mAh}/\text{cm}^2$ being harvested from coin cells after formation cycles in half-cells. High-loading Si anodes showed substantial mechanical degradation.

ding of high Si/pitch electrode loadings or similar macro-mechanical degradations observed in other Si-containing high loading electrodes is a necessary direction of future work for academic and industry groups to fully realize the energy density gains achievable when using Si-containing anodes.

Experimental Section

Synthesis of Si NPs. We used a custom nonthermal RF-enhanced plasma reactor first reported by Kortshagen and coworkers^[22] to produce the Si NPs. We have previously reported on the specific parameters used to produce different sized Si NPs,^[23] including the D50 = 5.9 nm Si NPs used herein.^[11] Briefly, SiH₄, Ar, and H₂ were flown through a 19 mm ID/25 mm OD quartz or alumina reactor tube at 20, 20, and 250 standard cubic centimeters per minute, respectively. The reactor maintained a capacitively-coupled plasma at 3 Torr between a copper ring electrode and grounded electrode positioned 10 mm downstream using an advanced Energy Cesar 136 generator applying 250 W of forward RF power at 13.56 MHz through an Advanced Energy VM1000 matching network (tuned to give a reflected power of 0–1 W). An Advanced Energy Z'scan device measured ~120 W delivered at the plasma over a reaction zone of approximately 60 cm³ for a plasma power density of ~2 W cm⁻³. The Si NPs formed in the plasma were collected downstream on a 400-mesh stainless steel screen and transferred air-free to an Ar glovebox.

Synthesis of Si/pitch active material. A petroleum pitch solution in toluene was prepared by first grinding pitch granules (Rain Carbon, 1 kg free sample, ZL 250 M gran.) in a mortar and pestle, dried under vacuum overnight, and transferred into an Ar glovebox. Pitch powder was added to toluene (Sigma-Aldrich, anhydrous, 99.8%) such that pitch comprised 20–30 wt.% of the pitch-toluene mixture. The mixture was stirred at ambient temperature for 2 days to dissolve the soluble pitch components, and the resulting slurry was vacuum filtered to remove the insoluble components. The pitch concentration of the filtrate was determined by evaporating the toluene from an aliquot, and a stock pitch solution was made by diluting the remaining filtrate to ~10 wt.% pitch in toluene. The 5.9 nm Si NPs (typically 5–10 g per batch) were mixed with the 10 wt.% pitch solution in toluene such that the Si to dissolved pitch was 50:50 by mass. The mixture was sonicated in an ultrasonic bath for 30 minutes to form a uniform slurry, which was then stirred under vacuum to evaporate the toluene to form monolithic chunks of Si/pitch solid. The Si/pitch solid was collected and transferred through air to a quartz boat and loaded into a tube furnace. The tube was sealed and the solid carbonized under 0.5 L/min N₂ flow by ramping the furnace up to 700 °C at 5 °C/min, dwelling for 1 h at 700 °C, then cooling sample to ambient temperature under continued N₂ flow. The carbonized Si/pitch was then transferred through air back to an Ar glovebox, minimizing the exposure time to air. The carbonized Si/pitch solid was then ball-milled at 500 rpm for 5 min with 12 × 8 mm ZrO₂ balls (Pulverisette 7 planetary micro mill premium line, 45 mL ZrO₂ milling jar). The resulting powder was then brushed through a 325-mesh sieve (45 µm opening) to yield the final Si/pitch active material powder used to make the electrodes.

Preparation of uncoated Si active material. The 5.9 nm Si NPs produced from the plasma reactor were treated before being processed into electrodes.^[24] Briefly, approximately 500 mg Si NPs were added to 3 mL of N-Methyl-2-pyrrolidone (NMP, Sigma-Aldrich, anhydrous, 99.5%) in an inert Ar atmosphere with 5 mg of 1,1'-azobis (cyclohexanecarbonitrile) as a radical initiator. The mixture was heated at 170 °C with stirring for 48 h before being

cooled. Toluene (5 mL) was added, the mixture centrifuged 12,500×g for 5 min, and the supernatant decanted from the precipitated Si NP pellet. This toluene washing procedure was repeated once more before the Si NPs were dried under vacuum. This procedure passivates the surface of the NPs with covalently bonded NMP molecules to allow the NPs to be processed normally in the electrode slurries.^[18] If this procedure is not performed prior to formulating the electrode slurry, the slurry will gel and be unable to print smoothly.

Slurry preparation and electrode casting. Si/pitch electrodes were prepared under an inert argon atmosphere using conventional slurry formulation and casting techniques. Typically, 8 mass equivalents of Si/pitch powder were ball-milled (same parameters as before) with 1 mass equivalent of Timcal C65 conductive carbon. A 10 wt.% solution of P84 polyimide (Teacapowder P84, Ensinger Sintimid GmbH) in NMP was then added to the Si/pitch + carbon mixture in a screwcap scintillation vial such that the final slurry comprised 80:10:10 by mass of each the Si/pitch powder, Timcal C65, and P84 polyimide, respectively. Glass beads were added to the slurry, and the slurry was mixed with a Mazerustar KK-250S planetary mixer before being cast onto the rough side of a Cu foil current collector using a doctor blade set to a 45 µm wet gap. The printed electrode was dried under vacuum at 150 °C for 4 hours, then underwent a subsequent 350 °C anneal for 4 h under 0.5 L/min of flowing nitrogen gas (see Figure S6 in the Supporting Information for data from electrodes tested without undergoing the additional 350 °C annealing step). The uncoated Si NP electrodes were produced using a similar procedure where the uncoated Si NPs, Timcal C65, and P84 polyimide binder solution were mixed together with the planetary mixer with a mass ratio of 80:10:10 before being printed and dried.

Active material and electrode soaking in electrolyte. Small amounts of uncoated Si NPs (4.36 mg) and Si/pitch powder (7.40 mg; different powder masses were used to maintain a consistent mass of Si between samples), as described above, were each placed in 1 mL polypropylene vials. To each vial was added 100 µL of 1.2 M lithium hexafluorophosphate (LiPF₆) in 3:7 ethylene carbonate:ethylmethyl carbonate + 3 wt% fluoro-ethylene carbonate electrolyte (GenF3), and the vials were then sealed with crimp caps lined with a PTFE septum. The vials were gently heated at 50 °C for 24 h. A similar procedure was followed with 58.2 mg (total mass) Si electrode and 28.1 mg Si/pitch electrode. The electrode compositions are described above. To measure the gases produced by chemical reactions between the Si material and electrolyte, the headspace of the vial was collected with a syringe and needle that punctured the PTFE septum. The gas sample in the syringe (8 mL) was then directly injected into the gas port of an Agilent 7890 B gas chromatograph (GC) equipped with a flame-ionization detector (FID); the FID was used in conjunction with a methanizer to facilitate the analysis of light oxide gases (CO, CO₂). GC-FID analysis was conducted using a proprietary column system optimized for the separation of electrolyte components (30 m × 0.25 mm; Wasson-ECE Instrumentation). The system was run with He as carrier gas at 1 mL/min with the following GC column oven program: a starting temperature of 40 °C was held for 3 min; the temperature was increased at a rate of 18 °C/min to 200 °C; and the final temperature of 200 °C was held for 5 min. The FID was operated at 200 °C with the methanizer temperature set at 450 °C; H₂ and air flows for the FID were set at 25 and 450 mL/min, respectively.

Half-cell assembly. The Si/pitch electrode was tested using 15 mm diameter circular punches assembled into 2032 coin cells. Half-cells were assembled using a 9/16" diameter punch of lithium metal foil pressed onto a 1 mm thick steel spacer as a counter electrode. The electrodes were separated by a 19 mm diameter circular punch of Celgard 2325, and 40 µL of GenF3 was added as the electrolyte. The

cell was sealed with a hydraulic crimper and allowed to rest for 4 hours at ambient temperature before running any electrochemistry. The half-cells used in the voltage hold experiment were rested for 4 h, then cycled at ambient temperature around 25 °C between 10–750 mV vs. Li/Li⁺ for three C/10 forming cycles with constant voltage holds at the voltage limits until the current relaxed to 1/30th of its initial value. On the 4th lithiation, the cells were held at a constant voltage of 10 mV for 180 h and the current was recorded. After the 180 h voltage hold, the cells were cycled an additional two C/10 cycles.

Full-cell electrochemical testing. The half-cells used for prelithiating the Si electrodes were rested for 4 h after assembly, then cycled between 10–750 mV vs. Li/Li⁺ for three C/20 forming cycles using a calculated 1 C current density of 2.36 mA/cm². After formation, the half-cell was disassembled and the Si/pitch electrode was recovered for reassembly into a full-cell with an additional 40 μL of fresh electrolyte. The 14 mm diameter circular cathode punch used in the full cell was provided by the Cell Analysis, Modeling and Prototyping (CAMP) facility at Argonne National Lab: Cathode A-C022, 90 wt % Targray NMC622, 5 wt % Timcal C-45, 5 wt % Solvay 5130 PVDF Binder, 9.78 mg/cm², ~1.49 mAh/cm². The full-cells were tested between 3–4.1 V using a 1 C current density of 1.5 mA/cm² of the cathode area. Separate Si/pitch electrodes formed in different half cells were used for each the rate capability and cycle lifetime tests.

Electron microscopy. Samples for transmission electron microscopy (TEM) were prepared by dipping a copper TEM grid with lacey carbon support film (Ted Pella) into a suspension of the Si/pitch powder dispersed in toluene via bath sonication. The grid was left to dry under a fume hood for at least 15 minutes before transferring to an FEI Tecnai ST30 TEM, operated at 300 kV, for imaging. Energy dispersive X-ray spectroscopy was performed on an FEI F20 scanning transmission electron microscope (S/TEM), operated at 200 kV in STEM mode, using the same sample preparation. Scanning electron microscopy images of the Si/pitch electrodes were collected on a Hitachi 4800 microscope with a 15 kV accelerating voltage and a working distance of approximately 10–12 mm.

Supporting Information

Supporting Information is available from the Wiley Online Library or from the author.

Author Contributions

M. C. Schulze: Synthesis and electrochemical performance testing of Si/pitch, original draft preparation. K. Fink and B. J. Tremolet de Villers: Electrolyte soaking and gas analysis, review and editing, contact bertrand.tremolet@nrel.gov regarding gas analysis. J. Palmer, C. Zweifel, C. Engtrakul: Gas analysis. G. M. Carroll: Preparation of uncoated Si material. N. S. Dutta: Electron microscopy. S. Han: Raman spectroscopy. N. R. Neale: Supervision.

Acknowledgements

This work was authored by the National Renewable Energy Laboratory (NREL), operated by Alliance for Sustainable Energy, LLC, for the U.S. Department of Energy (DOE) under Contract No. DE-AC36-08GO28308. This research was supported by the U.S. Department of Energy's Vehicle Technologies Office under the Silicon Consortium Project, directed by Brian Cunningham, and managed by Anthony Burrell and by the Laboratory Directed Research and Development (LDRD) Program at NREL. This work was also supported in part by the U.S. Department of Energy, Office of Science, Office of Workforce Development for Teachers and Scientists (WDTS) under the Science Undergraduate Laboratory Internships Program (SULI). The views expressed in the article do not necessarily represent the views of the DOE or the U.S. Government. The U.S. Government retains and the publisher, by accepting the article for publication, acknowledges that the U.S. Government retains a nonexclusive, paid-up, irrevocable, worldwide license to publish or reproduce the published form of this work, or allow others to do so, for U.S. Government purposes. Thanks to Cheyenne Paeppe at NREL for providing CHNOS elemental analysis.

Conflict of Interests

The authors declare no conflict of interest.

Data Availability Statement

The data that support the findings of this study are available from the corresponding author upon reasonable request.

Keywords: silicon nanoparticle anodes · pitch carbon-coating · lithium-ion batteries · carbonate-based electrolytes · high loading full-cells

- [1] a) M. N. Obrovac, V. L. Chevrier, *Chem. Rev.* **2014**, *114*, 11444–11502; b) Y. Jin, B. Zhu, Z. Lu, N. Liu, J. Zhu, *Adv. Energy Mater.* **2017**, *7*, 1700715; c) A. Du, H. Li, X. Chen, Y. Han, Z. Zhu, *Chem. Sel.* **2022**, *7*, e202201269.
- [2] H. Wang, S. Lu, X. Wang, S. Xia, H. Chew, *J. Phys. D* **2022**, *55*, 063001.
- [3] X. H. Liu, L. Zhong, S. Huang, S. X. Mao, T. Zhu, J. Y. Huang, *ACS Nano* **2012**, *6*, 1522–1531.
- [4] X. Su, Q. Wu, J. Li, X. Xiao, A. Lott, W. Lu, B. W. Sheldon, J. Wu, *Adv. Energy Mater.* **2014**, *4*, 1300882.
- [5] a) Y. Xu, K. Wood, J. Coyle, C. Engtrakul, G. Teeter, C. Stoldt, A. Burrell, A. Zakutayev, *J. Phys. Chem. C* **2019**, *123*, 13219–13224; b) J. E. Coyle, M. T. Brumbach, G. M. Veith, C. A. Apblett, *J. Phys. Chem. C* **2020**, *124*, 8153–8161; c) Y. Ha, B. J. T. De Villers, Z. Li, Y. Xu, P. Stradins, A. Zakutayev, A. Burrell, S. Han, *J. Phys. Chem. Lett.* **2020**, *11*, 286–291; d) C. Stetson, Y. Yin, A. Norman, S. P. Harvey, M. Schnabel, C. Ban, C. Jiang, S. C. Decaluwe, M. Al-jassim, *J. Power Sources* **2021**, *482*, 228946; e) R. T. Pekarek, A. Affolter, L. L. Baranowski, J. Coyle, T. Hou, E. Sivonxay, B. A. Smith, R. D. McAuliffe, K. A. Persson, B. Key, C. Apblett, G. M. Veith, N. R. Neale, *J. Mater. Chem. A* **2020**, *8*, 7897–7906; f) Y. Ha, C. Stetson, S. P. Harvey, G. Teeter, B. J. Tremolet de Villers, C. S. Jiang, M. Schnabel, P. Stradins, A. Burrell, S. D. Han, *ACS Appl. Mater. Interfaces* **2020**, *12*, 49573; g) C. Stetson, Y. Yin, C. S. Jiang, S. C. Decaluwe, M. Al-Jassim, N. R. Neale, C. Ban, A. Burrell, *ACS Energy Lett.* **2019**, *4*, 2770–2775; h) C. L. Seitzinger, R. L. Sacci, J. E. Coyle, C. A. Apblett, K. A. Hays, R. R.

- Armstrong, A. M. Rogers, B. L. Armstrong, T. H. Bennet, N. R. Neale, G. M. Veith, *Chem. Mater.* **2020**, *32*, 3199–3210; i) Y. Yin, E. Arca, L. Wang, G. Yang, M. Schnabel, L. Cao, C. Xiao, H. Zhou, P. Liu, J. Nanda, G. Teeter, B. Eichhorn, K. Xu, A. Burrell, C. Ban, *ACS Appl. Mater. Interfaces* **2020**, *12*, 26593–26600; j) T. F. Malkowski, Z. Yang, R. L. Sacci, S. E. Trask, M. F. Rodrigues, I. D. Bloom, G. M. Veith, *J. Power Sources* **2022**, *523*, 231021.
- [6] Y. He, L. Jiang, T. Chen, Y. Xu, H. Jia, R. Yi, D. Xue, M. Song, A. Genc, C. Bouchet-Marquis, L. Pullan, T. Tessner, J. Yoo, X. Li, J. G. Zhang, S. Zhang, C. Wang, *Nat. Nanotechnol.* **2021**, *16*, 1113–1120.
- [7] a) Q. Man, Y. An, C. Liu, H. Shen, S. Xiong, J. Feng, *J. Energy Chem.* **2023**, *76*, 576–600; b) G. Nava, J. Schwan, M. G. Boebinger, M. T. McDowell, L. Mangolini, *Nano Lett.* **2019**, *19*, 7236–7245; c) A. Alvarez Barragan, G. Nava, N. J. Wagner, L. Mangolini, *J. Vac. Sci. Technol. B, Nanotechnol. Microelectron. Mater. Process. Meas. Phenom.* **2018**, *36*, 011402.
- [8] H. Su, A. A. Barragan, L. Geng, D. Long, L. Ling, K. N. Bozhilov, L. Mangolini, J. Guo, *Angew. Chem.* **2017**, *129*, 10920–10925.
- [9] S. Chae, Y. Xu, R. Yi, H. Lim, D. Velickovic, X. Li, Q. Li, C. Wang, J. Zhang, *Adv. Mater.* **2021**, *33*, 2103095.
- [10] a) S. Jiang, B. Hu, R. Sahore, H. Liu, G. F. Pach, G. M. Carroll, L. Zhang, B. Zhao, N. R. Neale, Z. Zhang, *ACS Appl. Energ. Mater.* **2019**, *2*, 6176–6183; b) T. R. Martin, L. Ryneanson, M. Kuller, J. Quinn, C. Wang, B. Lucht, N. R. Neale, *Adv. Energy Mater.* **2023**, *13*, 2203921; c) M. C. Schulze, G. M. Carroll, T. R. Martin, K. Sanchez-Rivera, F. Urias, N. R. Neale, *ACS Appl. Energ. Mater.* **2021**, *4*, 1628–1636; d) M. C. Schulze, N. R. Neale, *ACS Energy Lett.* **2021**, *6*, 1082–1086.
- [11] M. C. Schulze, F. Urias, N. S. Dutta, Z. Huey, J. E. Coyle, G. Teeter, R. Doeren, B. J. Tremolet de Villers, S.-D. Han, N. R. Neale, G. M. Carroll, *J. Mater. Chem. A* **2023**, *11*, 5257–5266.
- [12] B. Apicella, A. Tregrossi, F. Stanzione, A. Ciajolo, C. Russo, *Chem. Eng. Trans.* **2017**, *57*, 775–780.
- [13] a) X. H. Liu, L. Zhong, S. Huang, S. X. Mao, T. Zhu, J. Y. Huang, *ACS Nano* **2012**, *6*, 1522–1531; b) Y. He, L. Jiang, T. Chen, Y. Xu, H. Jia, R. Yi, D. Xue, M. Song, A. Genc, C. Bouchet-Marquis, L. Pullan, T. Tessner, J. Yoo, X. Li, J. G. Zhang, S. Zhang, C. Wang, *Nat. Nanotechnol.* **2021**, *16*, 1113–1120.
- [14] C. L. Seitzinger, R. L. Sacci, J. E. Coyle, C. A. Appblett, K. A. Hays, R. R. Armstrong, A. M. Rogers, B. L. Armstrong, T. H. Bennet, N. R. Neale, G. M. Veith, *Chem. Mater.* **2020**, *32*, 3199–3210.
- [15] M. C. Schulze, M.-T. F. Rodrigues, J. D. McBrayer, D. P. Abraham, C. A. Applett, I. Bloom, Z. Chen, A. M. Colclasure, A. R. Dunlop, C. Fang, K. L. Harrison, G. Liu, S. D. Minteer, N. R. Neale, D. Robertson, A. P. Tornheim, S. E. Trask, G. M. Veith, A. Verma, Z. Yang, C. Johnson, *J. Electrochem. Soc.* **2022**, *169*, 050531.
- [16] L. Zhu, H. Hou, D. Zhao, S. Liu, W. Ye, S. Chen, M. Hanif, *Int. J. Electrochem. Sci.* **2015**, *10*, 9547–9555.
- [17] U. S. Department of Energy Vehicle Technologies Program, *United States Advanced Battery Consortium Battery Test Manual For Electric Vehicles, Revision 3.1*, **2015**.
- [18] M. C. Schulze, G. M. Carroll, T. R. Martin, K. Sanchez-Rivera, F. Urias, N. R. Neale, *ACS Appl. Energ. Mater.* **2021**, *4*, 1628–1636.
- [19] M. Luo, M.-T. F. Rodrigues, L. L. Shaw, D. P. Abraham, *ACS Appl. Energ. Mater.* **2022**, *5*, 5513–5518.
- [20] Y. Zheng, H. J. Seifert, H. Shi, Y. Zhang, C. Kübel, W. Pfleging, *Electrochim. Acta* **2019**, *317*, 502–508.
- [21] a) Y. Zheng, H. J. Seifert, H. Shi, Y. Zhang, C. Kübel, W. Pfleging, *Electrochim. Acta* **2019**, *317*, 502–508; b) H. Shi, X. Liu, R. Wu, Y. Zheng, Y. Li, X. Cheng, W. Pfleging, Y. Zhang, *Appl. Sci.* **2019**, *9*, 956; c) N. Dunlap, D. B. Sulias-Kern, P. J. Weddle, F. Usseglio-Viretta, P. Walker, P. Todd, D. Boone, A. M. Colclasure, K. Smith, B. J. Tremolet de Villers, D. P. Finegan, *J. Power Sources* **2022**, *537*, 231464.
- [22] L. Mangolini, E. Thimsen, U. Kortshagen, *Nano Lett.* **2005**, *5*, 655–659.
- [23] L. M. Wheeler, N. C. Anderson, P. K. B. Palomaki, J. L. Blackburn, J. C. Johnson, N. R. Neale, *Chem. Mater.* **2015**, *27*, 6869–6878.
- [24] G. M. Carroll, M. C. Schulze, T. R. Martin, G. F. Pach, J. E. Coyle, G. Teeter, N. R. Neale, *ACS Appl. Energ. Mater.* **2020**, *3*, 10993–11001.

Manuscript received: May 5, 2023

Revised manuscript received: June 28, 2023

Accepted manuscript online: June 29, 2023

Version of record online: July 25, 2023